https://doi.org/10.5194/nhess-2020-131
Preprint. Discussion started: 1 September 2020

Natural Hazards and Earth System Sciences Discussions
Open Access
EGU

Landslides distribution at tributaries with different evolution stages in Jiangjia Gully, southwestern China

Xia Fei Tian [a, b, c*], Yong Li [a, b], Quan Yan Tian [c, d]

a. Key Laboratory of Mountain Hazards and Surface Process, CAS, Chengdu, 610041, China
b. Institute of Mountain Hazards and Environment, CAS, Chengdu, 610041, China
c. University of Chinese Academy of Sciences, Beijing 100049, China
d. Cold and Arid Region of Environmental and Engineering Research Institute, CAS

*Corresponding author: Li Yong
E-mail: ylie@imde.ac.cn

Abstract: Landslide susceptibility assessment is of great significance for the disaster prediction and prevention. At present, most studies used statistical methods by the influence factors of landslide distribution, or based on physical models to determine the assessment result, the research of these methods was mainly focused on the gully scale. At the same time, these methods did not focus on the specific principle of material storage. In this paper, the surface erosion index, being the integral of the hypsometric curve, is adopted to explore the landslides distribution characteristic in different tributaries of the gully. Firstly, 81 tributaries of JJG are taken from DEM with 10 m grid cells, and the hypsometric curves are used to characterize their evolution stages; five stages are identified by the evolution index (EI, the integral of the hypsometric curves) and most tributaries are in relative youth stage with EI between 0.5 and 0.6. Then 906 landslides are interpreted from Quickbird satellite image of 0.61 m resolution. It is found that LD (LD = landslides number in a tributary/ the tributary area) increases exponentially with EI, while LA_p (LA_p = landslides area in a tributary/ the tributary area) fluctuates with EI, meaning that landslides are inclined to occur in tributaries with EI between 0.5 and 0.6, and thus these tributaries are the main material sources supplying for debris flows.

Key words: Hypsometric curve; Evolution stages; Tributaries; Landslides distribution

1 Introduction

https://doi.org/10.5194/nhess-2020-131
Preprint. Discussion started: 1 September 2020


Natural Hazards and Earth System Sciences
Discussions

Geomorphic evolution has been one of the important research topics in geomorphology, hypsometric analysis has been used to deal with erosional topography and the process of landform development (Bartolini et al., 2003; Li et al., 2011; Lv et al., 2005). Strahler (1952) asserted that different types of landform have different characteristic shape of their hypsometric curves, dividing landform into 'young' and 'mature' with the hypsometric integral decreasing. The integral can be used to indicate the geomorphological evolution state, in this meaning, it can be defined as the evolution index (EI) of a tributary (Kashani et al., 2019; Qureshi et al., 2019; Strahler, 1952, 1957). Meanwhile, the hypsometric curves are related to tributary form and erosional process, and are used to interpret landform development stages (Schumm, 1956; Strahler, 1952, 1957), which can represent the state of material storage of a tributary. In addition, the relationship between EI and tributary characteristics changes with scales. For example, the dissection index of tributaries presents various relationships to EI depending on scale of the tributaries. For the 5th-order tributaries, their correlation is r = 0.41, whereas for the 4th-order, it is r = 0.24, and it becomes negative correlation for the 3rd-order (Hamza et al., 2018). Combined with the results of field investigation, this study adopts the tributary scale that debris flow easily occurs to meet our research need.

The comprehensive analysis of various factors is equivalent to the black box theory, landslide susceptibility assessment over large areas is considered a preliminary step for the planning or design of the most appropriate risk mitigation measures. The use of statistics and physics based models is considered a useful tool for landslide susceptibility assessment (Amashi et al., 2019; Baena et al., 2019; Ciurleo et al., 2019; Hu et al., 2019; Rao et al., 2017; Singh et al., 2019; Xie et al., 2015). However, the research of these methods was mainly focused on the gully scale. At the same time, these methods did not focus on the specific principle of material storage, but statistical or comprehensive analysis on the main factors affecting the landslides distribution is carried out. While the integral of hypsometric curve is an index to represent the storage state of a tributary. Therefore, this paper uses the hypsometric curve integral to represent the storage state of a tributary. Compared with the comprehensive analysis, the hypsometric curve integral is a direct index from the tributary itself with material storage state.

For a given watershed, especially a small gully in mountains (below 100 km^2 and most below 10 km^2), the tributaries with different EI present various characteristics. Similarly, significant difference exists in the distribution of landslides among various tributaries, landslides are frequent in some tributaries while occasional in others (Baum et al., 2005; Pradhan and Sameen, 2017; Wang et al., 2006;

https://doi.org/10.5194/nhess-2020-131
Preprint. Discussion started: 1 September 2020


Natural Hazards and Earth System Sciences Discussions

Wieczorek, 1996). Therefore, the relationship between EI and landslides distribution has special significance to reveal the landslides distribution in tributaries, which, however, has been gotten little attention in literatures.

In this paper, a case study is conducted in the Jiangjia Gully (JJG), where weak and similar lithology, disparate topography, sparse vegetation, and unconsolidated deposits are widely distributed in tributaries. In addition, the debris flow behavior in JJG are representative, it is known for the high variety of debris flows; each debris-flow event consists of tens or hundreds surges of different flow regimes, velocities, discharges, and total volumes (Li et al., 2015; Li et al., 2013; Arai, 2017). In particular, the surges are composed of different materials, suggesting that they come from different sources (Xiang et al., 2015). In other words, each debris flow in JJG comes from different tributaries (Bollschweiler et al., 2007; Li et al., 2012; Li et al., 2013; Li et al., 2015). Generally, the flow surges are originated from different tributaries and the material supplies are mainly from landslides (including avalanches, soil failures and other slope processes) (Beguería, 2006). So the study of landslides distribution in different evolution stages is of great significance to reveal the landslides distribution characteristics of the tributaries, which can roughly determine the material supply and explain the formation mechanism of debris flow surges.

2 Study area and data collection

2.1 The setting of the study area

JJG is located in the Xiaojiang River of the Upper Changjiang River. The mainstream channel length is 1.39×10^4 m and the gully area is 4.84×10^7 m^2 (Fig. 1). This region undergoes active neotectonic movement, faults, and folds; and rocks are dominated by slate, dolomite, limestone, basalt and breccia rocks, which are easily weathered (Gabet and Mudd, 2006). The exposed strata in this gully is mainly shallow metamorphic rocks of the lower proterozoic Kunyang group, accounting for about 80% of the whole gully area (Wu et al., 1990). Generally, weak lithology, wide faults and sparse vegetation are the obvious characteristics of the gully, and the tributaries are in steep topography and intense landslide activity, with wide distribution of quaternary unconsolidated deposits. Loose materials are widely distributed in the gully and debris flows occur frequently, which are the major material sources for the debris flows. According to the statistics data, the landslides area reaches 16.4 km^2 that accounts for 39.7% of the gully area. As well, average annual sediment yield by debris flow is about 1.54×10^6 m^3 (Wu et al., 1990; Zhuang et al., 2015).

https://doi.org/10.5194/nhess-2020-131
Preprint. Discussion started: 1 September 2020

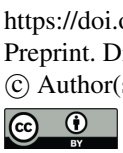

Natural Hazards and Earth System Sciences
Discussions

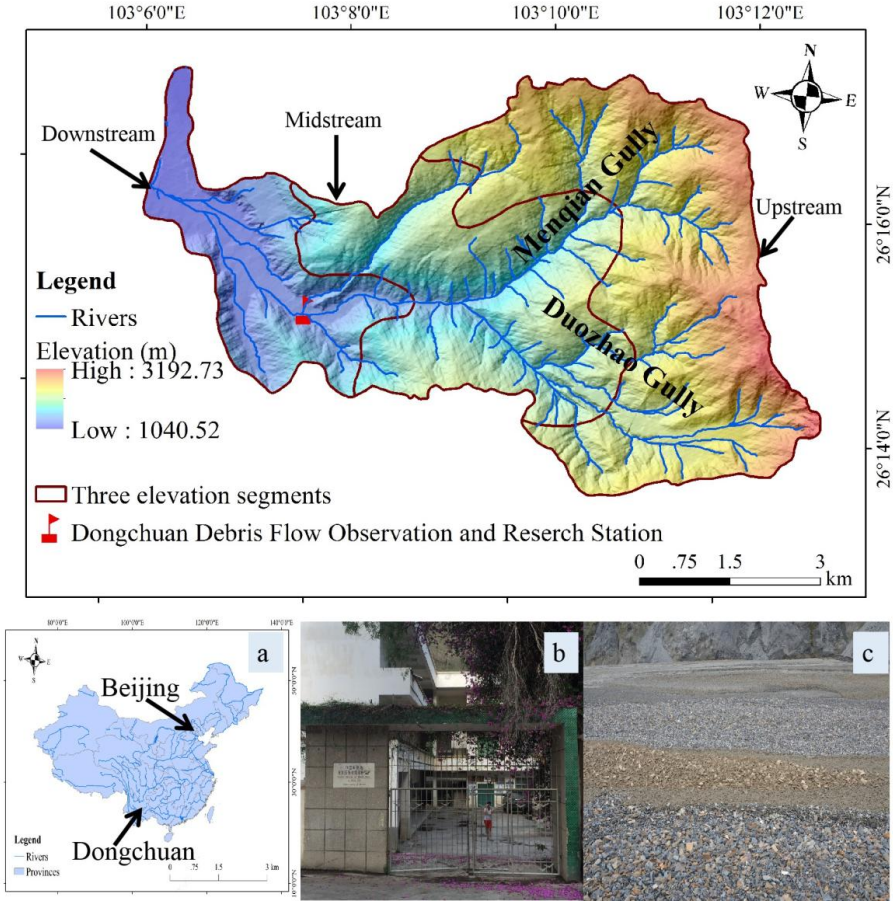

Fig. 1 The location of JJG. a The location of Dongchuan in China. b Dongchuan Debris Flow Observation and research stations. c Deposition of surges.

2.2 Data collection

2.2.1 The tributaries divided in JJG

Digital elevation model with spatial resolution 10 m is used in this study to generate elevation and area information, which was purchased in the Sichuan surveying and mapping bureau. 81 tributaries are abstracted from the watershed of JJG. The tributaries are divided based on field investigation result that each tributary is a complete unit for observable landslides and debris flows, also according to the fact that debris flows are prone to occur instead of direct extraction based on the same water collection threshold. In other words, these tributaries are all conspicuous in surface mass movement and loose materials are distinguishable on its slope. The tributaries are extracted from the DEM using GIS tool and also with artificial correction to ensure the accuracy of boundaries (now it is Fig. 3). In principle,

https://doi.org/10.5194/nhess-2020-131
Preprint. Discussion started: 1 September 2020

Natural Hazards and Earth System Sciences
Discussions

the gully can be divided further into smaller tributaries, but that makes little difference for the present purpose as to distinguish tributaries. Some tributaries in field are displayed in Fig. 2, obviously, there are significant differences among these tributaries The tributary area varies between $8.7 \times 10^4 \sim 2.07 \times 10^6$ m^2 and cover a total area of 4.62×10^7 m^2, about 95% of the whole gully. The serial number of tributary in subregions is presented in Table 1.

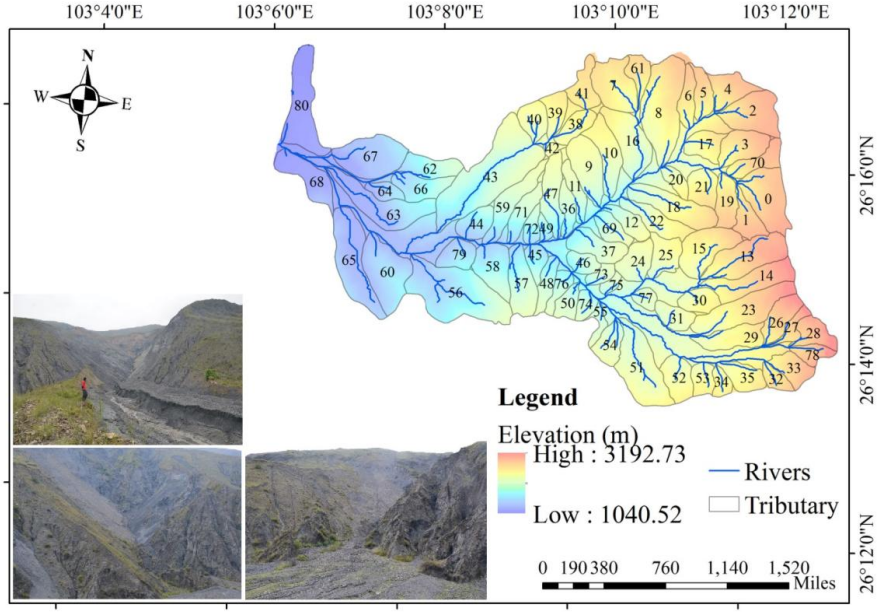

Fig. 2 The tributaries divided of JJG. Some tributaries in the field are shown on the map.

Table 1 The tributaries distribution in subregions.

Subregion	The No. of tributaries
Menqian Gully	2, 4, 5, 6, 7, 8, 9, 10, 11, 12, 16, 17, 18, 20, 22, 36, 37, 47, 49, 61, 69
Duozhao Gully	13, 14, 15, 23, 24, 25, 26, 27, 28, 31, 32, 33, 34, 35, 45, 46, 48, 50, 51, 52, 53, 54, 55, 73, 74, 75, 76, 77, 78
Upstream	0, 1, 2, 3, 4, 5, 6, 7, 8,10, 13, 14, 15, 16, 17, 19, 20, 21, 23, 26, 28, 29, 30, 32, 33, 34, 35, 38, 39, 40, 41, 42, 61, 70
Midstream	9, 11, 12, 22, 31, 36, 37, 43, 45, 46, 47, 48, 49, 50, 51, 54, 55, 59, 69, 71, 72, 73, 74, 75, 76, 77
Downstream	44, 56, 58, 60, 62, 63, 64, 65, 66, 67, 68, 79, 80

2.2.2 The hypsometric curve and EI

https://doi.org/10.5194/nhess-2020-131
Preprint. Discussion started: 1 September 2020


Natural Hazards and Earth System Sciences Discussions

Hypsometric curve for each tributary is calculated. The hypsometric curve is generated by plotting the relative area along the abscissa and the relative height along the ordinate. The relative height can be obtained as the ratio of the height of a given contour (h) from the base plane of the stream mouth to total height of the tributary with reference to the maximum elevation (H), and the relative area is obtained as the ratio of the area above a particular contour (a) to the total area of the tributary encompassing the outlet (A) (Strahler, 1952).

Hypsometric integral is the area between the hypsometric curve (y=h/H and x=a/A) and coordinate axis (Strahler, 1952, 1957), which can be defined as the evolution index (EI).

2.2.3 The extraction of landslides information

Quickbird image of 0.61 m resolution is purchased to create an inventory of landslides. The satellite image is adopted in this study with low cloud shadow coverage, and the aerial coverage of the cloudy area is 0.09 km^2 in the study area, about 0.18% of the gully. The atmospheric correction and radiometric correction have been carried out by using the calibration function within the tools of Envi 5.1 software, and 4, 3, 2 bands are combined to false color image stretched of contrast using standard deviation method. Both landslides number and landslides area are necessary to interpret, so the equal area projection is adopted, which has less impact on the landslides area. The landslides information becomes easily extracted on the source image after processing, which is beneficial to the work of visual interpretation, and thus ensures the accuracy of the results.

Landslides are mapped from high resolution satellite data acquired using visual image interpretation on Arc GIS 10.3 software with false color composites or panchromatic images uniformly on 1:5000 scale. The individual landslides initiation zones are indicated using polygons. In the case of complex situations where many landslides are interconnected, it is difficult to identify the individual initiation zones. Use of high resolution images enables demarcation of clustered landslides as individual polygons. The minimum size of landslides area extracted is determined as 253.26 m^2.

In the interpretation process, we make use of the following diagnostic features: the tone, texture, pattern and shape or form. Meanwhile, direct method, comparison method, integrated reasoning method and other synthetical methods are always used (Dai and Lee, 2002; Kumar et al., 2017; Valenzuela et al., 2017). Using the methods above, 906 landslides have been identified, with area ranging of $2.53 \times 10^2 \sim 6.7 \times 10^5$ m^2. In addition, fieldwork was carried out in May and June 2017. We investigated the location and area of 100 landslides distribution with the GPS instrument, and the

https://doi.org/10.5194/nhess-2020-131
Preprint. Discussion started: 1 September 2020

Natural Hazards and Earth System Sciences
Discussions
Open Access
EGU

accuracy achieves 89.21%. The LA (landslides area) and LN (landslides number) is obtained, they are used to analyze the relationship between EI with LA_p and LD of each tributary, of which LA_p is landslides area in a tributary/ the tributary area (%) and LD is landslides number in a tributary/ the tributary area (/10^6 m^2).

3 Evolution division of JJG

3.1 Hypsometric analysis

The hypsometric curves for tributaries are shown in Fig. 3:

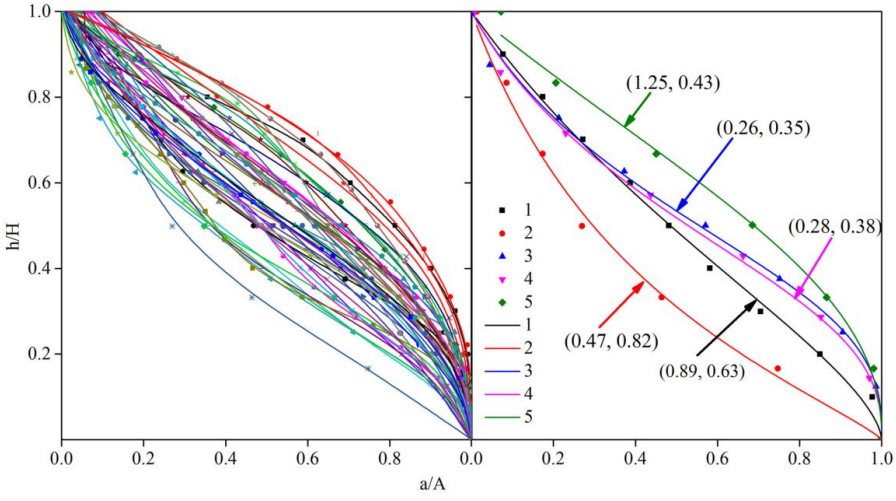

Fig. 3 The hypsometric curves of different tributaries.

The curves present various types, such as convex, concave and others between them; and these can be well fitted by the following function (Strahler, 1957):

$$y^{1/n}=k(1-x)/(x+k) \quad (1)$$

Where k and n are parameters, with the fitting coefficient R^2 of 0.90 and higher. It is found that higher the curve is, greater the k is. Meanwhile, the curve is rising as n decreases.

3.2 Evolution division of JJG

Then the EI of each tributary in JJG is calculated, which varies from 0.32 to 0.84. According to Strahler, there are three stages: inequilibrium or youthful stage (EI > 0.6), equilibrium or mature stage (EI between 0.3 and 0.6), and monadnock or old stage (EI < 0.3) (Strahler 1952). In order to distinguish the evolution differences of the tributaries, we conduct a more detailed classification and the EI of tributaries in JJG are divided into five groups (Fig. 4):

I (< 0.45), appears in downstream areas and near the outlet of the gully;

https://doi.org/10.5194/nhess-2020-131
Preprint. Discussion started: 1 September 2020

Natural Hazards and Earth System Sciences
Discussions

II (0.45-0.55), occurs mostly in the Duozhao Gully;

III (0.55-0.65), mostly distributes in midstream and downstream;

IV (0.65-0.75), mostly in midstream and upstream;

V (>0.75), mainly distributes in the headwaters of the Menqian Gully;

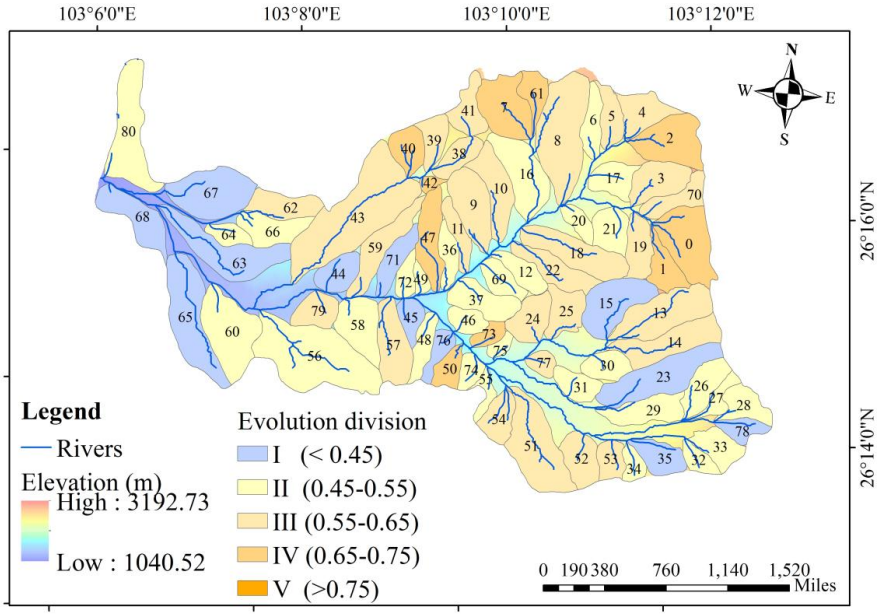

Fig. 4 The evolution division and EI distribution of tributaries in JJG.

Moreover, it is found that the EI satisfies the Weibull distribution with the scale parameter of 0.02 and the shape parameter of 1.69 (Fig. 5). The small value of scale parameter means that EI is much concentrated and EI of most tributaries in JJG is mainly between 0.5 and 0.6. The shape parameter is more than 1 and the frequency of the tributaries changes rapidly with the increasing of the EI, indicating that there is a great difference among the active tributaries. According to the frequency distribution of EI, the tributaries of JJG is generally in mature and youthful evolution stages, that is the reason why high frequency debris flow occurred in JJG in the past several decades.

https://doi.org/10.5194/nhess-2020-131
Preprint. Discussion started: 1 September 2020

Natural Hazards and Earth System Sciences
Discussions

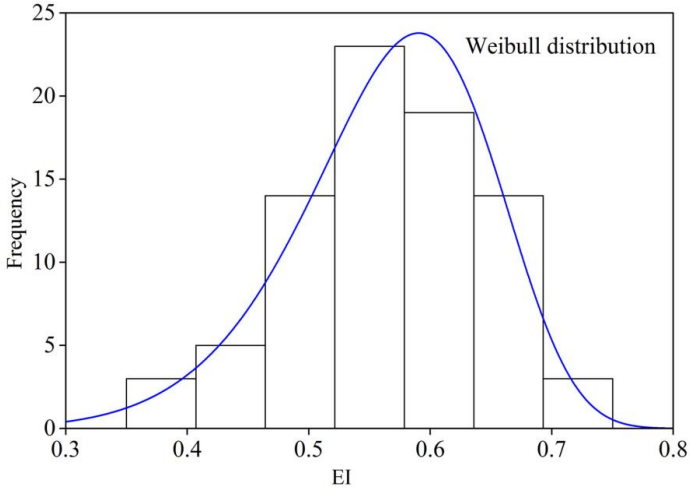

177

178 **Fig. 5** The frequency distribution of EI for tributaries in JJG.

179 3.3 Inflection point of hypsometric curves

180 Obviously, the hypsometric curves exhibit different shapes, which can be featured by the

181 inflection point, defined as the zero point of the second derivative of the fitting curve (Eq. 2):

182 $$y'' = \frac{nk^n(k+1)\,(2x+k-nk-n-1)\,(1-x)^{n-2}}{(x+k)^{n+2}} \quad (2)$$

183 where x denotes a/A, and y″=0 determines the inflection point at a/A_{ip}. It is found that the a/A_{ip} varies

184 with EI in a power law form (Fig. 6), meaning that the bigger the evolution index is, the lower the

185 inflection points of the curves are. The higher the EI value, the lower the inflection point, and this

186 implies that there should be more material accumulated in the lower part of the tributary, which are

187 relatively easy to join the the debris flow.

https://doi.org/10.5194/nhess-2020-131
Preprint. Discussion started: 1 September 2020

Natural Hazards and Earth System Sciences
Discussions

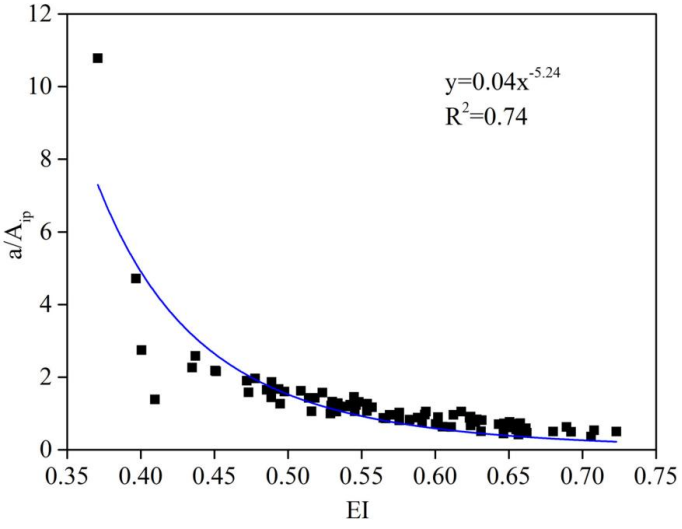

188

189 **Fig. 6** The relationship between the inflection point and and EI.

190 Moreover, we display the hypsometric curves of different evolution stages in Fig. 7; in particular,
191 the inflection points of the curves (the rectangle in each plot) are displayed in different position of the
192 curves. The inflection point indicates the elevation of a tributary with area varing. It can be seen in Fig.
193 7 that the larger of the EI is, the smaller of the a/A_{ip} is. When the point is high, the changing occurs at
194 the high elevation, i.e., mainly in the upstream of the tributary. Since there is no evolution area more
195 than 0.75 in JJG, four major evolution divisions are analyzed.

https://doi.org/10.5194/nhess-2020-131
Preprint. Discussion started: 1 September 2020

Natural Hazards and Earth System Sciences
Discussions

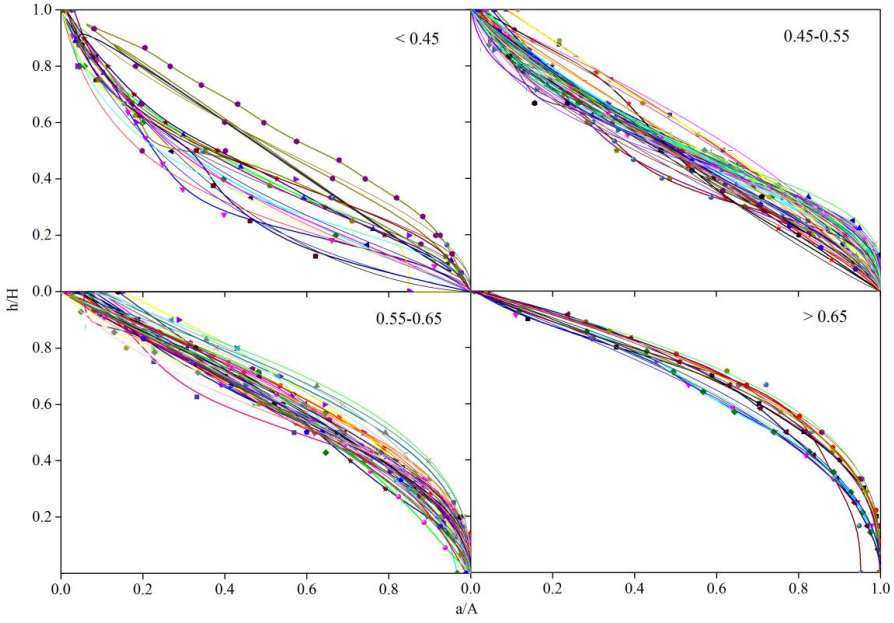

Fig. 7 Hypsometric curves of different EI divisions

The evolution curve changes from concave to convex with the increasing of evolution value, and the convex form of the tributary is more conductive to the material movement of the tributary and more loose materials are produced.

For a given elevation of point, larger area above means that more material are concentrated. For example, inflection points in EI between 0.45~0.55 are generally higher than those in EI below 0.45, indicating that more material concentrates in such tributaries, which are more prone to debris flow activities. Correspondingly, the lower the hypsometric curve is, the more concave the curve is presented, and the smaller the a/A_{ip} is, which indicates that the elevation changing in unit area is small, such a tributary is not conductive to the occurrence of landslides and debris flow activities.

Some landslides distribution of tributary in different evolutionary periods is shown in Fig. 8. In the tributary within the EI range of 0.35-0.45, the landslides distribution is scattered with the large area and low number, and the tributary is generally concave, which is not conductive to the materials movement. In addition, with the increasing of the evolutionary value, the landslides number is increasing and the area is decreasing, and the tributary in high EI division is convex, which is conductive to the materials movement.

https://doi.org/10.5194/nhess-2020-131
Preprint. Discussion started: 1 September 2020

Natural Hazards and Earth System Sciences
Discussions

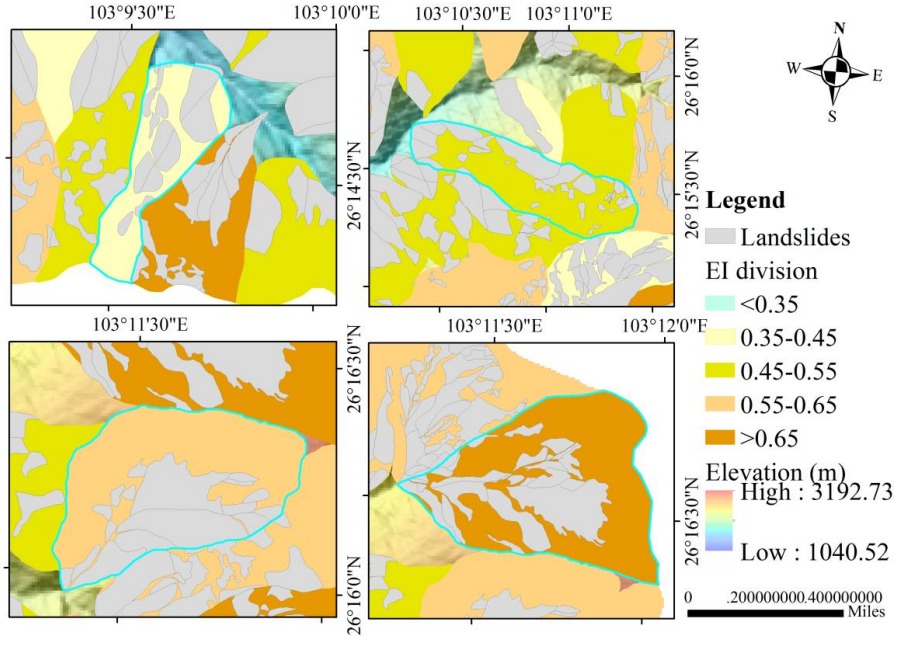

Fig. 8 Some landslides distribution tributaries of different EI divisions

4 Landslides distribution in relation to EI

4.1 Landslides distribution of JJG

A total of 906 landslides have been identified, with area ranging from 2.53 $\times 10^2$ m^2 to 6.7 $\times 10^5$ m^2. The spatial distribution of landslides is shown in Fig. 9.

https://doi.org/10.5194/nhess-2020-131
Preprint. Discussion started: 1 September 2020

Natural Hazards and Earth System Sciences
Discussions

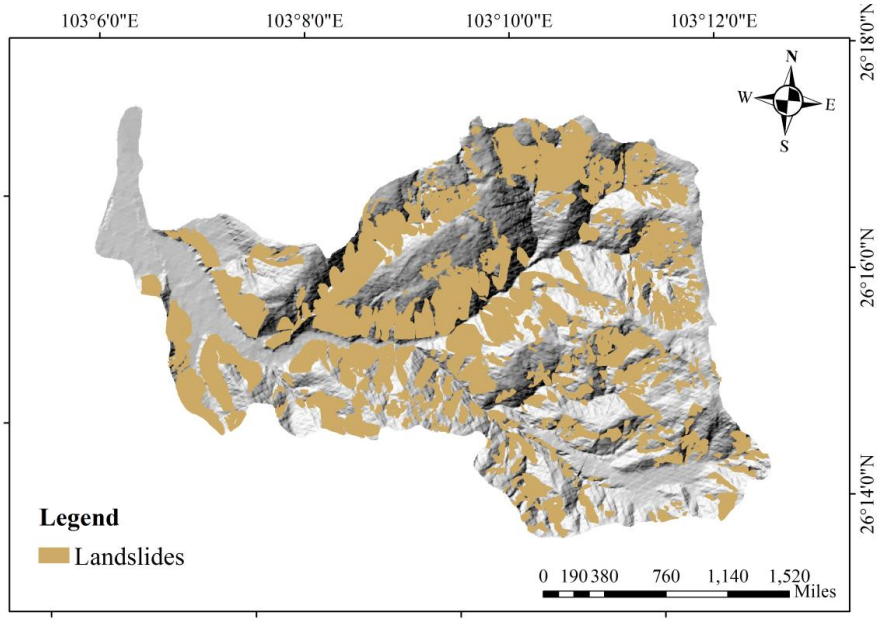

Fig. 9 Spatial distribution of landslides in JJG.

Landslides are mainly distributed in both sides along the mainstream channels. In details, landslides in Menqian Gully are more concentrated while in Duozhao they are scattering, which is consistent with field observations that landslides are always more frequent in clusters in vulnerable areas.

The landslides distribution in subregions is shown in Table 2. The area of the Menqian gully is smaller than Duozhao gully, the total area and number in Menqian gully is 4.78 km^2 and 274, respectively which is more than Duozhao gully with area 4.18 and number 232. In adddition, LA_p and LD in Menqian gully is more than in Duozhao gully. Since the area of the upstream is the largest and smallest in downstream, it is meaningless to compare the absolute value of the landslides. Now LA_p and LD in these segments is compared, and LA_p and LD are both greatest in upstream and smallest in downstream.

Table 2 The landslides distribution in subregions.

Subregion	The area	The area	Landslides			
	(km^2)	percentage (%)	LA (km^2)	LA_p (%)	LN	LD (km^{-2})
Menqian Gully	10.51	21.72	4.78	45.51	274	26

https://doi.org/10.5194/nhess-2020-131
Preprint. Discussion started: 1 September 2020

Natural Hazards and Earth System Sciences
Discussions

Duozhao Gully	11.16	23.05	4.18	37.51	232	21
Upstream	16.84	34.80	7.23	42.90	440	26.15
Midstream	10.48	21.65	4.13	39.40	261	25
Downstream	9.71	20.07	3.59	36.91	106	10.90

4.2 Landslides distribution in different evolution division

4.2.1 The landslides distribution related to evolution stages of all tributaries

The evolution division and landslides distribution layers are overlaid to form the spatial distribution map, as shown in Fig. 10. It is clear that major of landslides are distributed in subregions of III and IV, with EI between 0.55 ~ 0.75.

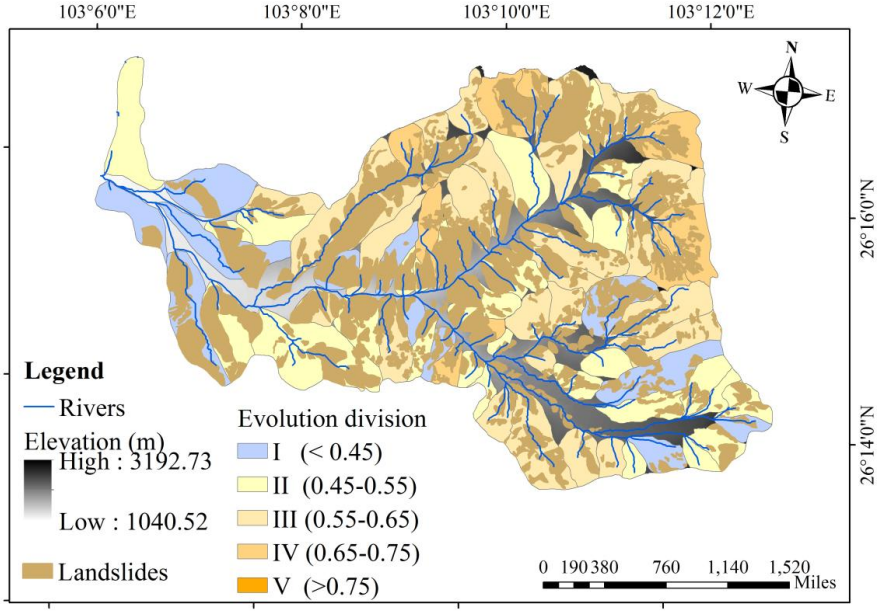

Fig. 10 Landslides distribution in various evolution stages.

Fig. 11 shows how LD and LA_p vary with EI. It shows that LD increases exponentially with EI increasing, which means that more landslides occur in the tributaries at younger stage. Meanwhile, the greater fluctuation of LA_p is in tributaries with the range of EI less than 0.55, while a smaller fluctuation is in tributaries of EI more than 0.55, and the LA_p is generally smaller than other evolution stages in active evolution stage.

https://doi.org/10.5194/nhess-2020-131
Preprint. Discussion started: 1 September 2020

Natural Hazards and Earth System Sciences
Discussions

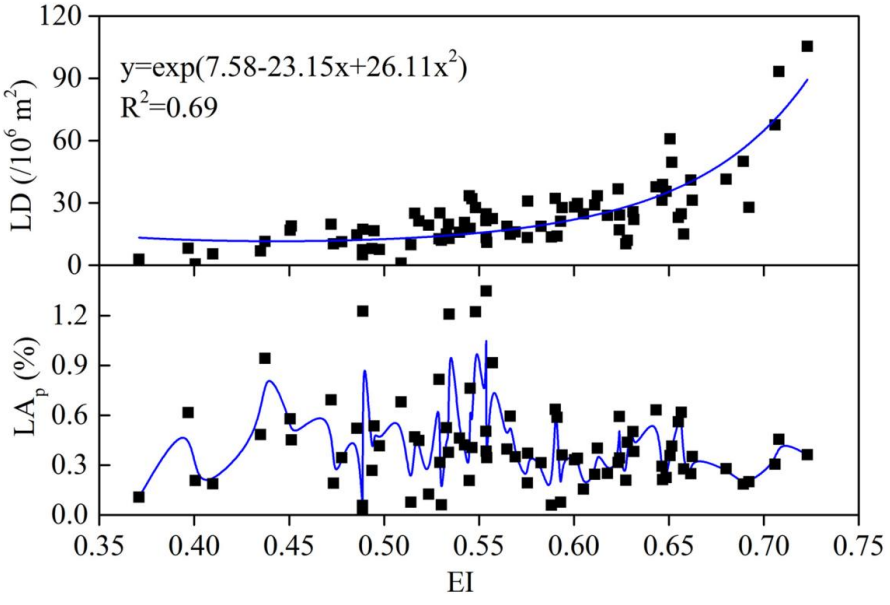

Fig. 11 Relationship between landslides and EI.

4.2.2 Landslides distribution in typical subregions

The major branches of JJG, the gully of Menqian and Duozhao, are distinctive in debris flow and landslides activities. As mentioned above, landslides are more scattering in Duozhao and more concentrated in Menqian. Now we consider how landslides distribute in tributaries in these subregions.

Fig. 12 shows that in both gullies LD increases exponentially with EI, almost in the same exponential function. As for LA_p, several peaks occur in different EI values in Menqian Gully but only a single peak occurs (around EI with 0.55) in Duozhao Gully, meaning that landslides are widely distributed in tributaries with EI >0.45 in Menqian Gully.

https://doi.org/10.5194/nhess-2020-131
Preprint. Discussion started: 1 September 2020

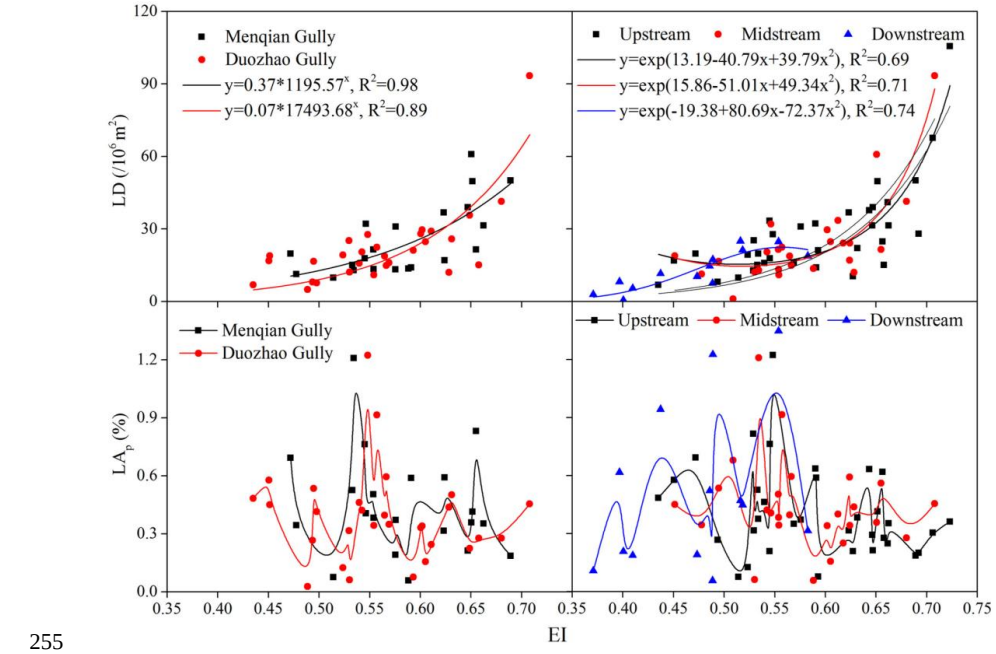

Fig. 12 Relationship between landslides and EI in subregions.

Similarly, we consider LD and LA_p in the regions of the upstream, midstream and downstream in JJG that have visible terrain difference, as shown in Fig. 12. Again it is found that LD increases exponentially with EI both in the upstream and midstream.

LA_p mainly increases first and then decreases as EI increases, and the LA_p-EI curve in the range of less than 0.54 is higher than the range of more than 0.54, which has the similar tendency with the LA_p-EI curve in all tributaries of JJG. Also the LA_p in upstream and midstream is higher than upstream, lower LA_p exists in tributaries at the younger evolutionary stages. Meanwhile, lower LD and larger LA_p is in the downstream, which is at the old evolution stage, which means that with the occurrence of historical landslides or large landslides in slope surface, the tributary has reached a stable state.

5 Discussion

5.1 The Power-law distribution of landslides

Power-law frequency-magnitude relationship has been generally observed for landslides at a wide range of size (Hovius et al., 1997; Stark and Hovius, 2001; Malamud et al., 2010), but for a small-scale gully like JJG there is no report in literatures. For the landslides in JJG, the power law is perfectly valid (Fig. 13), with exponent being -1.45, which differs much from the exponent for landslides over large

https://doi.org/10.5194/nhess-2020-131
Preprint. Discussion started: 1 September 2020

Natural Hazards and Earth System Sciences
Discussions

scale regions, such as those in the Gorkha area (2.5), the Northridge, California (2.30), and the Wenchuan area (2.19), and many other regions (Eeckhaut et al., 2007; Lari et al., 2014). The verification of power law confirms that the landslides area interpreted is reliable.

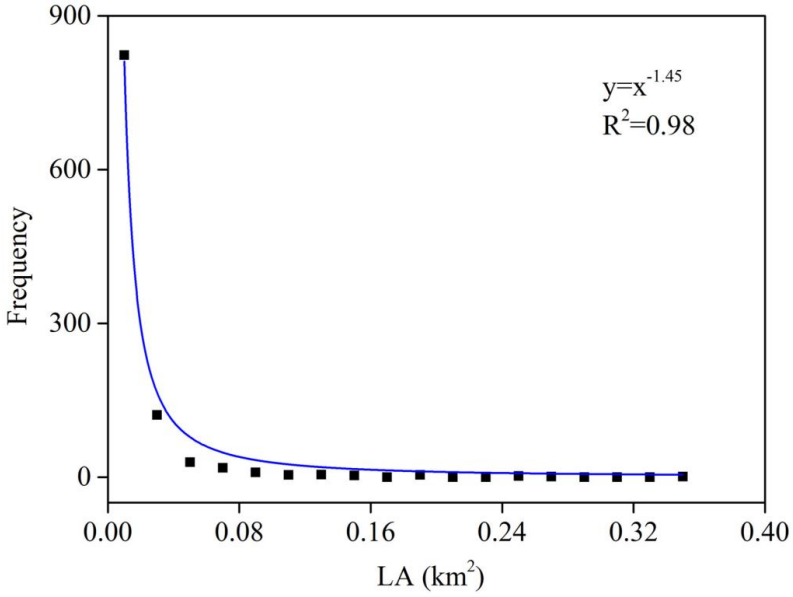

Fig. 13 The landslide area frequency distribution of JJG.

5.2 EI and tributary morphological feature

As a comprehensive topography index, EI reflects the geomorphology characteristics of the tributary. Fig. 14 shows how slope varies with EI on average, as it is crucial for landslides and debris flow formation. The maximal average slope, usually bigger than the friction angle of the soil, occur mainly between EI of 0.5-0.65, this coincides with range of most landslides distribution, and this also accounts for the relationship between EI and LD which indicates that EI is related to the number or frequency of landslides. Meanwhile, the landslides are concentrated in tributaries of class III (EI = 0.55~0.65), and these tributaries are concentrated in the midstream and upstream, mainly in the Menqian Gully. The landslides distribution in tributaries of different EI quantitatively reveals spatial heterogeneity distribution. The spatial distinction of landslides distribution results from the diverse evolution stages of tributaries, which provides a heterogeneous background for material supplying in gully. The spatial heterogeneity distribution can reveal the reason why landslides are frequent in some tributaries while occasional in others, thus roughly to predict the landslides activity of tributaries, which is of great significance to the comprehensive management of small watershed.

https://doi.org/10.5194/nhess-2020-131
Preprint. Discussion started: 1 September 2020

Natural Hazards and Earth System Sciences
Discussions

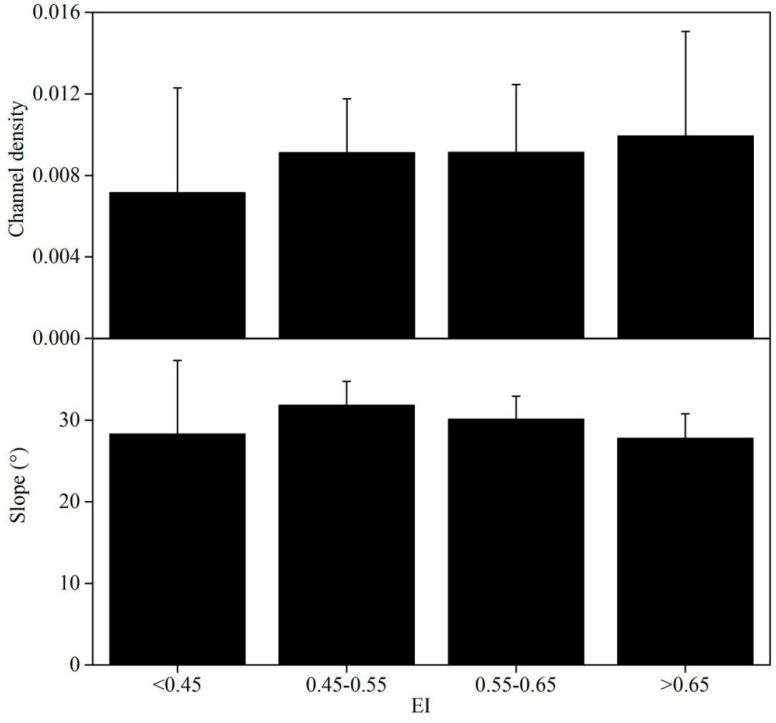

291

292 **Fig. 14** The variation of the tributary morphological feature in different evolution stages.

293 Debris flow converging from tributaries into mainstream channel depends on the flow routes, or
294 the stream length of each tributary, and this can be described by the channel density (i.e., the length in
295 unit area of a region). Fig. 15 shows the density variation with EI, indicating that the channel density of
296 tributary is increasing as EI rises, which is conducive to the occurrence of debris flow activity.

297 Then the tributaries of EI between 0.5 and 0.65 provide favorable condition both for landslides
298 and flow convergence, and thus facilitate the forming and developing of debris flows.

299 5.3 Implication in debris flow surges

300 The most remarkable features of debris flow in JJG are the high frequency in occurrence and great
301 variety of flow regime and magnitude. Each occurrence contains tens to hundreds of surges (Li et al.,
302 2012); the surges are separated in time and space, and different from one another in density, velocity,
303 and sediment concentration. The variation of flow velocity with density is shown in Fig. 15, which
304 contains surges in one single event on July 12, 2017.

305 The great variety of surges densities, with different material compositions, can be attributed to
306 different sources; this means that even a single surge material comes from different tributaries in most

https://doi.org/10.5194/nhess-2020-131
Preprint. Discussion started: 1 September 2020

Natural Hazards and Earth System Sciences
Discussions

cases (Webb et al., 1989). As observed in the last decades, debris flows almost come from the north branch, the Menqian Gully, while the south branch, the Duozhao Gully, is often silent. This presents the gross distinction of material and landslides activities in JJG, which further implies that there must be more differences in tributaries.

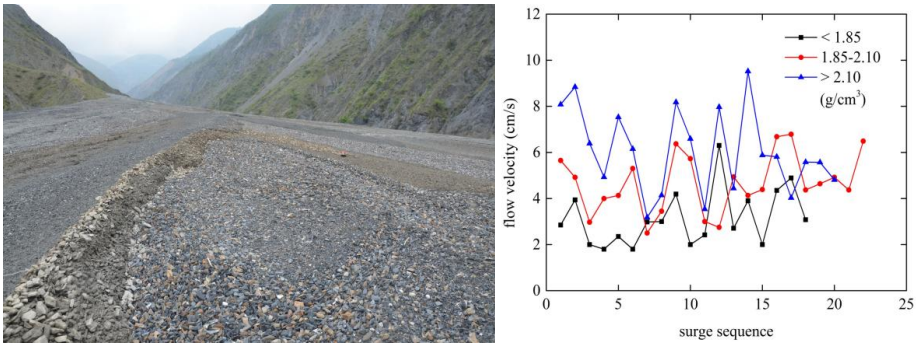

Fig. 15 Debris flow surges deposit in the mainstream of JJG.

The spatial heterogeneity of tributary distribution reveals the variety of debris flow sources. As it is difficult to observe the debris flows of each tributary, we usually see the convergence debris flows from multiple sources. Debris flow surges always present the characteristic of diverse forms from the perspective of material supplies (Li et al., 2015), and this can be attributed to the spatial heterogeneity of evolution and landslides activity of tributaries as discussed above.

Previous studies usually consider debris flows activity on the gully scale and ignore the distinction on tributary scale (Chen and Wang, 2017; Malet et al., 2004), they cannot tell the feature of debris flows from multiple sources and undergoing diverse tributaries processes, such as initiation on slope, flow downwards in tributary channel, and confluence into the mainstream, all closely related to the tributary feature.

Besides, the formation of debris flow is activated by rainfall (Chen et al., 2006; Fuchu et al., 1999; Fusco et al., 2017; Kuo and Chuan, 2007; McArdell et al., 2007; Reneau and Dietrich, 1987; Tan and Han, 1992), different rainfall intensity and amount is in different tributaries, which adds more diversity to the surges. The factor of precipitation will be the next study to consider and understand the formation mechanism of debris flow surges.

5.4 General application of EI for landslide source identification

The case study in JJG provides a relationship between EI and landslides distribution; the

https://doi.org/10.5194/nhess-2020-131
Preprint. Discussion started: 1 September 2020


Natural Hazards and Earth System Sciences
Discussions

traditional methods make a comprehensive analysis of various influencing factors of landslides (Amashi et al., 2019; Baena et al., 2019; Ciurleo et al., 2019; Hu et al., 2019; Rao et al., 2017; Singh et al., 2019; Xie et al., 2015), ignoring the landslides distribution mechanism itself, while this paper focuses on the analysis of the landslides distribution state itself in tributary, so this method can be generally applied to identify landslide sources in more general cases. For example, the Wenchuan earthquake has about 11,000 individual landslide points (Gorum et al., 2011), and it is found that these landslides are distributed mainly in relatively high EI tributaries (Tian et al., 2019; Xiang et al., 2015). The EI values for the landslide sources are also subject to the Weibull distribution (Fig. 16), which is similar to the case of JJG. In comparison, in JJG, EI of tributaries satisfies the Weibull distribution with the scale and shape parameter for JJG case are respectively of 0.02 and 1.69, while for, this is comparable to the EI distribution of tributaries in the Wenchuan region where the scale and shape parameter is 0.53 and 11.73, respectively. The scale parameter can reflect the EI range of variation, which varies between 0.38 and 0.64 in the Wenchuan area and betweenem 0.37 and 0.73 in JJG. The difference here can be attributed that a number of tributaries in JJG having no landslides, while in Wenchuan, only tributaries having landslides distribute in almost every tributary are taken into account, which means the concentration of EI. This also implies that landslides occur in tributaries within a relatively narrow range of EI. More important point is the difference between shape parameters, the bigger shape parameter in Wenchuan region means that the curve is to the right more than in JJG, implying that the earthquake is inclined to induce more landslides in tributaries of big EI. As JJG is of tributaries with wide range evolution stages, we choose it as the study area to reveal the mechanism of landslides distribution.

https://doi.org/10.5194/nhess-2020-131
Preprint. Discussion started: 1 September 2020

Natural Hazards and Earth System Sciences
Discussions

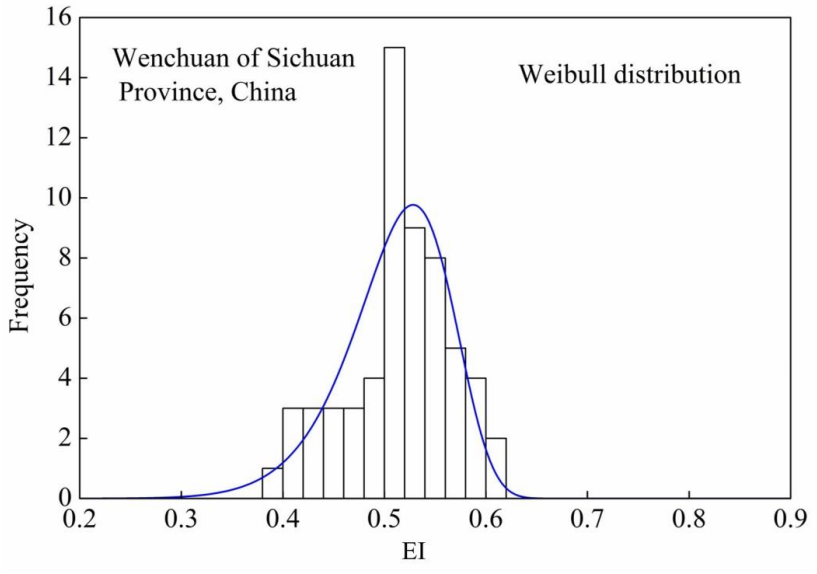

Fig. 16 The EI frequency distribution of Wenchuan in Sichuan province.

6 Conclusions

This study has revealed the spatial heterogeneity of landslides distribution in tributaries of different evolution stages. It is found that most landslides are distributed in the relative young tributaries (with evolution index between 0.5 ~ 0.6). Generally, the LD increases exponentially with EI and the LA_p is concentrated in EI between 0.5 and 0.6, in accordance with the general landslides distribution. The spatial heterogeneity of landslide distribution provides the background for the high variety and intermittency of debris flows in JJG.

Meanwhile, the EI satisfies the Weibull distribution, such distribution feature also occurs in the tributaries of landslides induced by the Wenchuan earthquake. This implies that the EI can be taken as an indicator for identifying landslide sources in mountainous watersheds.

Acknowledgments

This research is supported by the Strategic Priority Research Program of the Chinese Academy of Sciences (Grant No.XDA23090202) and the Key International S&T Cooperation Academy of Sciences (grant no. 2016YFE0122400).

References

https://doi.org/10.5194/nhess-2020-131
Preprint. Discussion started: 1 September 2020

370 Amashi, A. R., Hulagabali, A. M., Solanki, C. H., Solanki, G. R., and Dodagoudar.: Landslide Risk
371 Assessment and Mitigation—A Case Study. Conference paper 2019.
372 Arai, M.: A research on unsteady period of debris flow surges. EGU General Assembly Conference
373 Abstracts 19, 10715, 2017.
374 Baena, J. A. P., Scifoni, S., Marsella, M., Gianfilippo, D. A., and Clemente, I. F.: Landslide
375 susceptibility mapping on the islands of Vulcano and Lipari (Aeolian Archipelago, Italy), using a
376 multi-classification approach on conditioning factors and a modified GIS matrix method for areas
377 lacking in a landslide inventory. Landslides 2019.
378 Bartolini, C., D'Agostino, N., and Dramis, F.: Topography, exhumation, and drainage network
379 evolution of the apennines. Episodes 26, 212-216, 2003.
380 Baum, R. L., Coe, J. A., Godt, J. W., Harp, E. L., Reid, M. E., Savage, W. Z., Schulz, W. H., Brien, D.
381 L., Chleborad, A. F., and McKenna, J. P.: Regional landslide-hazard assessment for seattle,
382 washington, USA. Landslides 2, 266-279, 2005.
383 Beguer á, S.: Changes in land cover and shallow landslide activity: A case study in the spanish
384 pyrenees. Geomorphology 74, 196-206, 2006.
385 Berger, C., McArdell, B. W., and Schlunegger, F.: Sediment transfer patterns at the illgraben catchment,
386 switzerland: Implications for the time scales of debris flow activities. Geomorphology 125,
387 421-432, 2011.
388 Blahut, J., Westen, C. J. V., and Sterlacchini, S.: Analysis of landslide inventories for accurate
389 prediction of debris-flow source areas. Geomorphology 119, 36-51, 2010.
390 Bollschweiler, M., Stoffel, M., Ehmisch, M., and Monbaron, M.: Reconstructing spatio-temporal
391 patterns of debris-flow activity using dendrogeomorphological methods. Geomorphology 87,
392 337-351, 2007.
393 Chen, C. Y., and Wang, Q.: Debris flow-induced topographic changes: Effects of recurrent debris flow
394 initiation. Environmental monitoring and assessment 189, 449, 2017.
395 Chen, H., Dadson, S., and Chi, Y. G.: Recent rainfall-induced landslides and debris flow in northern
396 taiwan. Geomorphology 77, 112-125, 2006.
397 Ciurleo, M., Mandaglio, M. C., and Moraci, N.: Landslide susceptibility assessment by TRIGRS in a
398 frequently affected shallow instability area. Landslides 16(1):175-188, 2019.
399 Dai, F., and Lee, C.: Landslide characteristics and slope instability modeling using gis, lantau island,

https://doi.org/10.5194/nhess-2020-131
Preprint. Discussion started: 1 September 2020

400 hong kong. Geomorphology 42, 213-228, 2002.
401 Eeckhaut, M. V. D., Poesen, J., Govers, G., Verstraeten, G., and Demoulin, A.: Characteristics of the
402 size distribution of recent and historical landslides in a populated hilly region. Earth & Planetary
403 Science Letters 256, 588-603, 2007.
404 Fuchu, D., Lee, C., and Sijing, W.: Analysis of rainstorm-induced slide-debris flows on natural terrain
405 of lantau island, hong kong. Engineering Geology 51, 279-290, 1999.
406 Fusco, F., Allocca, V., and Vita, P. D.: Hydro-geomorphological modelling of ash-fall pyroclastic soils
407 for debris flow initiation and groundwater recharge in campania (southern italy). Catena 158,
408 235-249, 2017.
409 Gabet, E. J., and Mudd, S. M.: The mobilization of debris flows from shallow landslides.
410 Geomorphology 74, 207-218, 2006.
411 Gorum, T., Fan, X. M., Westen, C. J. V., Huang, R. Q., Xu, Q., Tang, C., and Wang, G. H.: Distribution
412 pattern of earthquake-induced landslides triggered by the 12 May 2008 Wenchuan earthquake.
413 Geomorphology 133(3-4):0-167, 2011.
414 Hamza, V., Prasannakumar, V., and Pratheesh, P.: Landform evaluation through hypsometric
415 characterisation: an example from selected river basin in southern western ghats, india 73, 4,
416 2018.
417 Hovius, N., Stark, C. P., and Allen, P. A.: Sediment flux from a mountain belt derived from landslide
418 mapping. Geology 25, 231-234, 1997.
419 Hu, M., Liu, Q., and Liu, P.: Susceptibility Assessment of Landslides in Alpine-Canyon Region Using
420 Multiple GIS-Based Models. Wuhan University Journal of Natural Sciences 24(3):257-270, 2019.
421 Huggel, C., Clague, J. J., and Korup, O.: Is climate change responsible for changing landslide activity
422 in high mountains? Earth Surface Processes and Landforms 37, 77-91, 2012.
423 Wu, J. s., Kang, Z. C., Tian, L. Q., and Zhang, S. C.: Debris flow observation in jiangjia gully, Yunnan
424 1990.
425 Kashani, R., Partabian, A., and Nourbakhsh, A.: Tectonic implication of geomorphometric analyses
426 along the Saravan Fault: evidence of a difference in tectonic movements between the Sistan
427 Suture Zone and Makran Mountain Belt. Journal of Mountain Science 16(05):78-89, 2019.
428 Kumar, D., Thakur, M., Dubey, C. S., and Shukla, D. P.: Landslide Susceptibility Mapping &
429 Prediction using Support Vector Machine for Mandakini River Basin, Garhwal Himalaya, India.

https://doi.org/10.5194/nhess-2020-131
Preprint. Discussion started: 1 September 2020

430 Geomorphology 295, 2017.
431 Kuo, L., and Chuan, T.: Progress in research on debris flow hazard assessment. Journal of
432 Catastrophology 1, 023, 2007.
433 Langebein, W. B., and Basil, W.: Topographic characteristics of drainage basins. USGS Water Supply
434 Paper 947-C, 1947.
435 Lari, S., Frattini, P., and Crosta, G. B.: A probabilistic approach for landslide hazard analysis.
436 Engineering Geology 182, 3-14, 2014.
437 Li, Y., Su, P. C., and Su, F. H.: Debris flow as a spatial poisson process. Journal of Mountain Science
438 29, 586-590, 2011 (In Chinese).
439 Li, Y., Liu, J. J., Hu, K. H., and Su, P. C.: Probability distribution of measured debris-flow velocity in
440 jiangjia gully, yunnan province, china. Natural hazards 60, 689-701, 2012.
441 Li, Y., Zhou, X. J., Su, P. C., Kong, Y. D., and Liu, J. J.: A scaling distribution for grain composition of
442 debris flow. Geomorphology 192, 30-42, 2013.
443 Li, Y., Liu, J. J., Su, F. H., Xie, J., and Wang, B. L.: Relationship between grain composition and debris
444 flow characteristics: A case study of the jiangjia gully in china. Landslides 12, 19-28, 2015.
445 Lv, X. J., Liu, X. L., and Su, P. C.: The Area-altitude Analysis on the Evolution Stage of Debris Flow
446 Ravines :Taking Daqu River as an Example. Journal of Mountain Science 23, 336-341, 2005 (In
447 Chinese).
448 Malet, J. P., Maquaire, O., Locat, J., and Rema îre, A.: Assessing debris flow hazards associated with
449 slow moving landslides: methodology and numerical analyses. Landslides 1, 83-90, 2004.
450 Martha, T. R., Roy, P., Mazumdar, R., Govindharaj, K. B., and Kumar, K. V.: Spatial characteristics of
451 landslides triggered by the 2015 m w, 7.8 (gorkha) and m w, 7.3 (dolakha) earthquakes in
452 nepal. Landslides 1-8, 2016.
453 McArdell, B. W., Bartelt, P., and Kowalski, J.: Field observations of basal forces and fluid pore
454 pressure in a debris flow. Geophysical Research Letters 34, 248-265, 2007.
455 Malamud, B. D., Turcotte, D. L., Guzzetti, F., and Reichenbach, P.: Landslide inventories and their
456 statistical properties, Earth Surface Processes & Landforms 29, 687-711, 2010.
457 Pike, R. J., and Wilson, S. E.: Elevation-relief ratio, hypsometric integral, and geomorphic area-altitude
458 analysis. Geological Society of America Bulletin 82, 1079-1084, 1971.
459 Pradhan, B., and Sameen, M. I.: Landslide susceptibility modeling: Optimization and factor effect

https://doi.org/10.5194/nhess-2020-131
Preprint. Discussion started: 1 September 2020

460 analysis. Laser scanning applications in landslide assessment, Springer 115-132, 2017.
461 Qureshi, J., Mahmood, S. A., Masood, A., Khalid, P., and Kaukab, I. S.: DEM and GIS-based
462 hypsometric analysis to study tectonics and lithologies in southern Suleiman fold and thrust belt
463 (Balochistan–Pakistan). Arabian Journal of Geosciences 12(5):144, 2019.
464 Rao, J., Shen, J., Tang, X. B., and **FU**, **X**. D.: Risk Assessment of Landslide Based on Fuzzy
465 Comprehensive Evaluation and Information Entropy. Journal of Yangtze River Scientific Research
466 Institute 2017.
467 Reneau, S. L., and Dietrich, W. E.: The importance of hollows in debris flow studies; examples from
468 marin county, california. Reviews in engineering geology 7, 165-180, 1987.
469 Schumm, S. A.: Evolution of drainage systems and slopes in badlands at Perth Amboy, New Jersey[J].
470 Bulletin of the Geological Society of America 67, 597-646, 1956.
471 Singh, A., Kanungo, D. P., and Pal, S.: Physical vulnerability assessment of buildings exposed to
472 landslides in India. Natural Hazards 2019.
473 Strahler, A.: Hypsomic analysis of erosional topography. Bulletin of Geol. Soc. of America 63,
474 1117–1142, 1952.
475 Stark, C. P., and Hovius, N.: The characterization of landslide size distributions. Geophysical Research
476 Letters 28, 1091-1094, 2001.
477 Strahler, A. N.: Quantitative analysis of watershed geomorphology. Eos, Transactions American
478 Geophysical Union 38, 913-920, 1957.
479 Tan, W. P., and Han, Q. Y.: Study on regional critical rainfall indices of debris flow in Sichuan province.
480 Journal of catastrophology 7, 37-42, 1992.
481 Tian, X. F., Su, F. H., Zhang, J. Q., Liu, J. J., and Li, Yong.: Frequency distribution of landslides in the
482 Wenchuan earth quake area. Journal of Mountain Science.
483 Valenzuela, P., Domínguez-Cuesta, M. J., García, M. A. M., and Jiménez-Sánchez, M.: A
484 spatio-temporal landslide inventory for the NW of Spain: BAPA database. Geomorphology 293,
485 11-23, 2017.
486 Wang, C., Esaki, T., Xie, M., and Qiu, C.: Landslide and debris-flow hazard analysis and prediction
487 using gis in minamata–hougawachi area, japan. Environmental Geology 51, 91-102, 2006.
488 Webb, R. H., Pringle, P. T., and Rink, G. R.: Debris flows from tributaries of the colorado river, grand
489 canyon national park, arizona. United States Geological Survey, Professional Paper 1492, 1989.

https://doi.org/10.5194/nhess-2020-131
Preprint. Discussion started: 1 September 2020

Natural Hazards and Earth System Sciences
Discussions

490 Wieczorek, G. F.: Landslide triggering mechanisms. Landslides: Investigation and mitigation 247,
491 76-90, 1996.
492 Wieczorek, G. F., and Glade, T.: Climatic factors influencing occurrence of debris flows. Debris-flow
493 Hazards and Related Phenomena. Springer Berlin Heidelberg, pp. 325-362, 2005.
494 Wu, J., Kang, Z., Tian, L., and Zhang, S.: Observation and research of debris flow in Jiangjiagou
495 Ravine, Yunnan Province. Science Pressing, Beijing, pp. 67–145, 1990.
496 Xiang, L. Z., Li, Y., Chen, H. K., Su, F. H., and Huang, X.: Sensitivity analysis of debris flows based
497 on basin evolution. Resources and environment of the Yangtze river basin 24, 1984-1992, 2015 (In
498 Chinese).
499 Xie, X., Wei, F., Zhang, J., and Shi, Y.: Application of Projection Pursuit Model to Landslide Risk
500 Classification Assessment. Earth Science 2015.
501 Zhuang J. Q., Cui, P., Wang, G. H., Chen, X. Q., and Guo, X. J.: Rainfall thresholds for the occurrence
502 of debris flows in the Jiangjia Gully, Yunnan Province, China. Engineering Geology 195, 335-346,
503 2015.